Energy Technology
Generation, Conversion, Storage, Distribution

Accepted Article

Title: Electric Field Poling Effect on the Electrocatalytic Properties of Nitrogen-Functionalized Graphene Nanosheets

Authors: Maryam Jahan, Kuo Li, and Guang-Lin Zhao

To be cited as: *Energy Technol.* 10.1002/ente.201800327

Link to VoR: http://dx.doi.org/10.1002/ente.201800327

www.entechnol.de

WILEY-VCH

Electric Field Poling Effect on the Electrocatalytic Properties of Nitrogen-Functionalized Graphene Nanosheets

*Maryam Jahan, Kuo Li, and Guang-Lin Zhao**

* To whom correspondence should be addressed. Email: guang-lin_zhao@subr.edu

AUTHOR ADDRESS: Physics Department and Nano Catalysts Laboratory, Southern University and A&M College, Baton Rouge, Louisiana, 70813, USA

KEYWORDS: N-doped Graphen, Electric field poling, Electrocatalyst, Oxygen Reduction Reaction

***Abstract*:** Fuel cells are attractive new technologies for producing sustainable and green energy. However, the high cost of its components such as Pt electrocatalyst is a major challenge. Heteroatom doped carbon nano-materials show potential applications for oxygen reduction reaction (ORR) which can be used for fuel cells and may be promising replacement of Pt catalyst. Recently, we implemented a facile method for preparing partially nitrogen functionalized graphene oxide (PNG) nano-sheets. To achieve better nitrogen functionalization, graphene oxide was annealed in ammonia solution for 12 h at 220^{o}C. The electrochemical measurement data show that the PNG synthesized in NH_3 environment possesses good electrocatalytic activities for ORR. In addition, we identified a physical method for the first time to drive the randomly oriented graphene nano-sheets to be aligned parallel to the surface of electrode for electrocatalytic application by using an AC electric field. An additional effect of the applied electric field is the induction of a polarization on PNG nano-sheets that create a dielectrophoresis phenomenon. The poling effect of the electric field on the sample shows much improved electrocatalytic performance. The enhanced catalysis can be used for ORR as an important reaction in fuel cells. The reported new method can achieve a low cost capability for preparing new electrocatalyst electrodes for large-scale applications.

1. Introduction

Rapid depletion of fossil fuels increased attention for alternative energy sources to meet the growing energy demand. Fuel cells can convert sustainable energy carriers (e.g., renewable hydrogen or bio-gas) into electrical power and heat. Microbial fuel cells (MFCs) are environmentally friendly technology which converts chemical energy stored in waste-waters directly into electrical energy by using microorganisms as biocatalysts. However, the overall low power density of the MFC and the high cost of components are two major issues for its commercialization. Therefore, environmentally friendly and low-cost oxygen reduction reaction (ORR) electrocatalysts have been considered for fuel cells including MFCs. Platinum (Pt) catalysts have outperformed all other catalysts in areas such as activity, stability, and selectivity and have dominated the fuel cell applications as the preferred ORR catalysts. However, high cost and low availability of Pt catalyst increased the overall cost of industrial scale application of fuel cells. Therefore, environmentally friendly and low-cost catalysts are considered as an attractive alternative to Pt catalyst. Considering green chemistry, graphene has attracted intense scientific interest in recent years due to its extraordinary properties. [1-3] The fantastic electronic properties of graphene are related to its unusual electron band structure, i.e., a zero band gap with nearly linear dispersion bands that touch at the Dirac point.[4] In addition, the charge carrier mobility in graphene is very high.[5,6] When graphene sheets are placed randomly on a substrate, they tend to form irreversible agglomerates or restack due to the strong π–π stacking and van der Waals interactions, hindering the potentials that could be offered by individual graphene sheets. Control over the

orientation or arrangement of a nanostructure can provide advantages and additional leverage for certain applications. For example, oriented one–dimension (1D) nanomaterials, such as carbon nanotubes (CNTs), can outperform non-oriented counterparts in some applications such as electrocatalyst for oxygen reduction reaction (ORR).[7] When an electrical potential is applied between a CNT arrays, high local electric fields can be produced through nanotubes. Similarly, when the orientation of graphene on a substrate is changed from randomly oriented to being highly oriented to the substrate surface, it can more effectively harvest the intrinsic properties of graphene.

Up to now, researchers have used different approaches for orienting carbon nano-materials to be used as fillers in polymer based composites by employing mechanical stretching,[8] an electric field,[9,10] or a magnetic field.[11-13] The use of an electric field has been reported to align carbon nanotubes,[9,10] carbon nanofibers,[14] carbon black,[15] and graphene sheets[16,17] to improve the electrical conductivity and mechanical properties of polymer nanocomposites by aligning the material in the matrix. Kim et al. developed epoxy nanocomposites with graphite having average diameter of 10 μm and a maximum diameter of 50 μm, aligned along the alternating-current (AC) electric field direction.[18,19] The glass-fiber and graphite chains arranged in epoxy are parallel to the electric field.[19] Chen et al. prepared polyester resin nanocomposites with graphite nanosheets oriented by the applied AC electric field, and found that the electrical conductivity was greatly increased in the alignment direction. [20-22] They showed that graphite sheets were oriented with their flakes parallel to the electric field.[20]

In this work, we prepared partially nitrogen-functionalized graphene oxide nano sheets named as PNGs afterwards. Further, we studied the electrocatalytic properties of the PNGs after applying an AC electric field to the sample drop-casted on a glassy carbon electrode. The previous studies using electric field to align graphene sheets along the electric field in polymeric composites,[20-22] focused on their thermo-physical responses[19] or the optical properties of the field-induced composite film.[17] Here, we used electric field to align graphene nanosheets which are perpendicular to the electric field for enhancing electrocatalytic performance of the material.

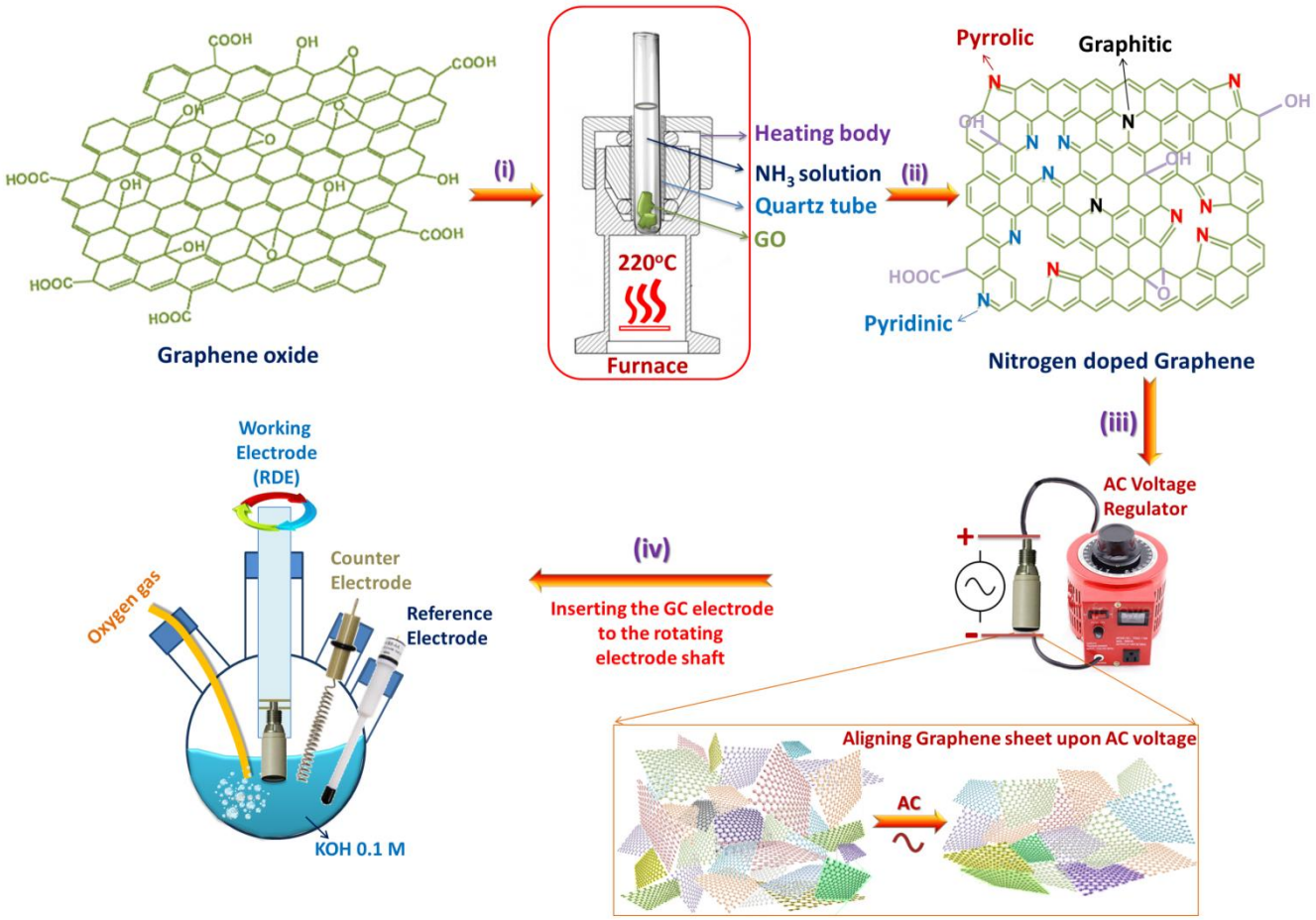

Figure 1. Schematic illustration for the sample preparation procedure.

(i) The solution of graphene oxide mixed with ammonia solution and then transferred to a quartz tube;
(ii) The mixture heated at 220°C for 12 h;
(iii) The collected powder mixed with Nafion solution and ethanol to make a catalyst ink. The ink drop casted onto a GC electrode. Then the electrode was inserted between two AC electrodes (the gap between the AC electrode and the surface of electrode sample was 1.5 mm), followed by applying AC voltage to PNGs drop casted on GC electrode.
(iv) After applying AC electric field, the catalyst ink on the GC electrode dried, and the interchangeable electrode was inserted in a RDE measurement instrument for ORR measurement in alkaline solution

To the best of our knowledge, this is the first report which presents the results of the electric field poling effect on the electrocatalytic properties of partially nitrogen functionalized graphene oxide sheets (PNGs) using an external AC electric field. Applying the electric field also causes a Columbic attraction force between PNGs due to the polarization of graphene sheets decorated with charged functional groups. The electrostatic attraction forces are recruited to assist in the packing of the PNGs layers. Efficient packing created by stronger bonding interactions produced a closely packed surface of the electrocatalyst electrode to exhibit an improvement in the conductivity. The closely packing arrangement of PNGs has not been seen in previous reports.

We have achieved the improvement in the electrocatalytic performance of the sample through the measurements of electrochemical properties regarding ORR after applying AC electric field. Since ORR plays a vital rule in various applications including hydrogen fuel cells, lithium-air batteries, gas sensors, our noble-metal-free catalysts have potential applications as a promising replacement of the currently used precious metal (such as Pt) catalysts.

2. Experimental

2.1. Material Preparation Procedures

50 mg commercial graphene oxide (GO) obtained from Sigma Aldrich was added in 5 mL deionised (DI) water and sonicated for 60 min to disperse well. Afterwards, 33 mL

Ammonia solution (25-28 wt% in water) was added and dispersed by conventional stirring. The solution was then transferred to a quartz tube to heat for 12 hours at 220 ^{o}C inside an oven. The synthesized powder of partially nitrogen-functionalized graphene oxide sheets (PNGs) was collected by centrifugation and desiccation at 80^{o}C overnight in a vacuum oven to remove the physisorbed NH_3. Then the catalyst ink from the PNG powder was added on a glassy carbon (GC) electrode. Further, the electrode with PNG ink was inserted between two AC electric electrodes and an AC electric filed was applied till the catalyst ink completely dry. Figure 1 shows the schematic procedure for the sample preparations and the experimental apparatus used to apply an AC electric field to the electrocatalyst ink. The AC electric field was applied using two parallel electrodes. An AC voltage was supplied between 0 to 120 V using an AC voltage transformer with a constant frequency of 60 Hz. The gap between the AC electrode and the surface of electrode sample was 1.5 mm. After the catalyst ink dried under the electric field, the interchangeable working electrode was then inserted into the electrode shaft of rotating disk electrode (RDE) measurement instrument, followed by measuring the electrochemical properties of electrocatalysts for oxygen reduction reaction.

2.2. Characterizations

For all samples, scanning electron microscopy (SEM) images were taken with (JSM-6610LV, JOEL. Japan, at voltage 15 kV) equipped with energy-disperse secondary analysis system (EDS) (EDAX, USA). The microstructures of the samples were characterized by using transmission electron microscopy (TEM) at 120 KV (JEM-1400, JEOL, Japan). For TEM studies, a drop of sonicated material suspension in ethanol was placed on a 3 mm copper grid, followed by drying under ambient conditions.

Kratos Axis 165 X-ray photoelectron spectrometer (XPS)/Auger electron spectroscope were used to measure XPS spectra. The samples were studied by the XPS photoelectron spectroscopy using Al Kα 1486.6 eV x-ray. High resolution spectra of C-1s, N-1s and O-1s regions were also collected on the samples. During data acquisition runs, pass energy of 160 eV, current at 10 mA and a time of 20 ms per step were used.

2.3. Electrochemical Measurements.

To prepare the catalyst for electrochemical measurements, 10 milligrams of the synthesized sample was mixed with the following solution: 1.25 mL ethanol solution and 50 µl Nafion (5 wt%). This solution was sonicated for 1 h to achieve homogenous ink. Then a 10 µl drop of the catalyst ink was loaded onto the polished surface of the GC disk (d = 5 mm) and dried slowly at room temperature to achieve a uniform surface. Once the sample was completely dried, we estimated the amount of the sample delivered to the surface at ~400 µg/cm^2. The sample was then used in electrochemical experiments immediately after drying. Finally, commercial catalyst 20 wt. % Pt/C was used as comparisons and prepared in the same way to achieve a similar loading of 400 µg/cm^2 of 20 wt% Pt/C (Pt loading : 80 µg/cm^2).

All measurements were carried out at room temperature using a potentiostat (A-METEC) with a three-electrode electrochemical cell. RDE measurements were performed on a Pine instrument. We used an interchangeable GC disk electrode with a 5 mm diameter as the working electrode, a platinum (Pt) wire as the counter electrode, and Hg/HgO (in KOH solution) as the reference electrode. Linear sweep voltammetry (LSV) measurements were performed in O_2-saturated 0.1 M KOH solutions at a scan rate of 10 mVs^{-1}. The cyclic voltammetry (CV) experiments were conducted typically at a scan rate of 50 mV s^{-1}. RDE measurements were performed at rotation rates of 1600 rpm, with the scan rate of 10 mV s^{-1}. For applying an electric field using an AC voltage from 0 V to 120 V at room temperature, our GC electrode surface was facing AC field electrodes with a spacing of 1.5 mm between the electrodes. For the sample exposed to the electric field by using for example 80 V, the electric field was 53.3 V/mm. So we name the sample as PNGs [53.3 V/mm] afterwards, here the value in the brackets refers to the applied electric field strength.

2.4. Calculation of differential conductance for the samples:

We also implemented a computational method to calculate the differential conductance *(dJ/dV)* of the sample from the electrochemical measurement data of electric current density, *J*. A third order numerical differentiation method was used as follows, [23]

$$\frac{dJ}{dV} = \frac{(\Delta J_3 - 9 * \Delta J_2 + 45 * \Delta J_1)}{60 * h}$$

Where $\Delta J_1 = J(V + h) - J(V - h)$;

$\Delta J_2 = J(V + 2h) - J(V - 2h)$;

$\Delta J_3 = J(V + 3h) - J(V - 3h)$;

and h is the step size between the two data points of the potential (V) in the calculation.

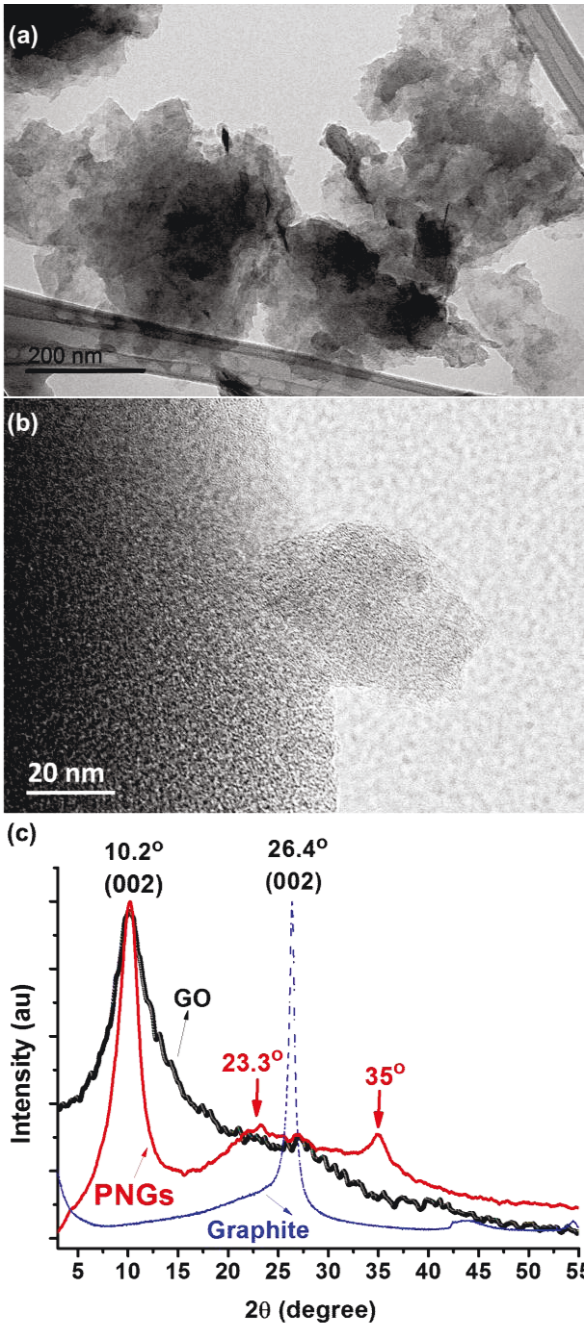

Figure 2 (a) TEM image of PNGs; (b) High resolution TEM image of PNGs ; (c) XRD patterns of GO, PNGs, and graphite.

3. Results and discussion

3.1. Characterization of the sample

Figure 2 (a) and (b) show the TEM images of the PNG sample. The presence of graphene sheets in the sample after doping with nitrogen can be seen.

The XRD spectra in Figure 2(c) show the interlayer variations and the crystalline properties of graphite, GO, and PNGs. Graphite shows a very sharp diffraction peak at 2θ=26.4°, corresponding to the interlayer (002) spacing of 0.34 nm. After oxidation, the interlayer (002) spacing corresponded to the diffraction peak of 10.2° increased to 0.86 nm for GO, which is much larger than that of pristine graphite owing to the introduction of oxygen-containing functional groups on the surface of graphene sheet[24] and atomic scale roughness arising from structural defects (sp^3 bonding).[25] Since the majority of PNGs are made of GO, we can also see a sharp peak around 10.2° in the sample. After doping with the ammonia mixture solution, another peak at 23.3° was ascribed to the partial reduction of GO and the exfoliation of the layered GO nanosheets.[26] Another diffraction peak around 35° in the sample can be seen in Figure 2(c). Similarly, Ouyang et al. observed a small peak at around 35° in the XRD data of nitrogen-doped graphene which is due to the presence of nitrogen in the graphene sample. [27]

The study for the presence of nitrogen (1.75% nitrogen content) after doping was performed by XPS and the data was shown in Figure 3(a), since it has been shown that nitrogen doping in carbon nanostructures can improve their electrocatalytic activity.[28-30] XPS spectra of C1s binding energy (BE) were shown in Figure 3(b), indicating sp^2 C (284.7 eV), sp^3 C (284.9 eV), C-O/ C-N (286.2 eV), and π excitation (290.7 eV). We can see from the XPS spectra of O1s BE in Figure 3(c), which shows O1: O–C (531.5 eV), O2: O=C (532.4 eV), O3: O–C=O (534.1 eV).[31] Figure 3(d) shows the XPS spectra of functionalized graphene in N1s BE range. The XPS spectra are fitted to get detailed chemical bonding information of the elements N and O with carbon. Nitrogen is observed in N-graphene sheet confirming its incorporation into graphene. Generally, there are several nitrogen functional groups in nitrogen-functionalized carbon structure. These include pyridinic-N (N1, BE = 396.1 eV), pyrrolic-N (N2, BE = 400.2 eV), quaternary nitrogen (N3, BE = 401.9 eV), and N-oxides of pyridinic-N (N4, BE = 403.2 eV).[32-34] The nitrogen functional groups are usually in the following molecular structures (chemical states):[32-34] pyridinic-N (labelled as N1) refers to nitrogen atoms at the edge of graphene planes, each of which is bonded to two carbon atoms and donates one π-electron to the aromatic π-system; pyrrolic-N (labelled as N2) refers to nitrogen

atoms that are bonded to two carbon atoms and contribute to the p system with two π-electrons; quaternary nitrogen (labelled as N3) is also called ''graphitic nitrogen'' or ''substituted nitrogen'', in which nitrogen atoms are incorporated into the graphene layer and replace carbon atoms within a graphene plane; N-oxides of pyridinic-N (labelled as N4, pyridinic–(N+ – O)) are bonded to two carbon atoms and one oxygen atom. The role of the real ''electrocatalytically active sites'' is still controversial since their contribution to the catalytic activity is not well defined.[30] In some studies, the enhanced electrocatalytic activity is attributed to pyridinic-N and/or pyrrolic-N. [32-34]

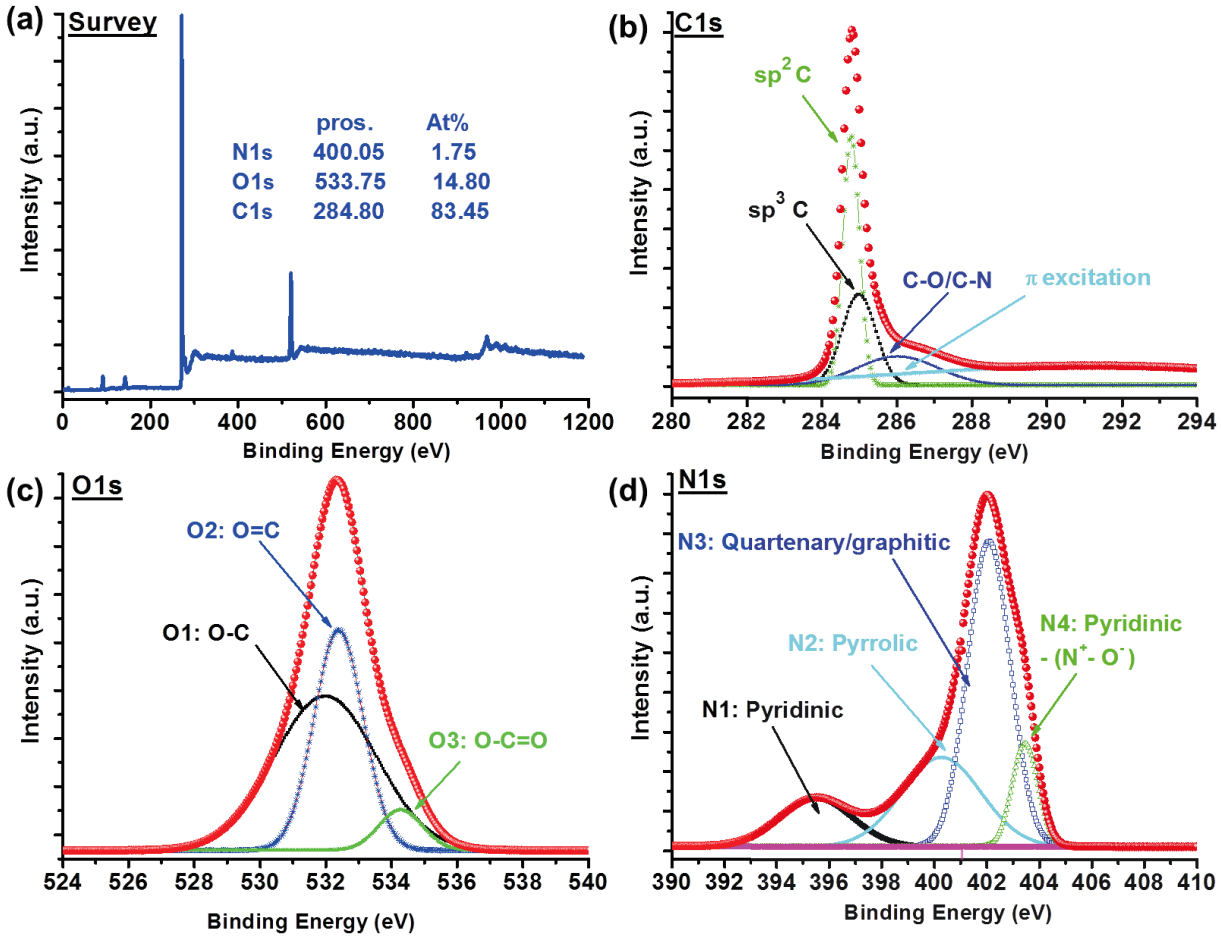

Figure 3. **(a)** XPS survey , (b) C1s, (c) O1s , and (d) N1s spectra of PNGs.

Miyata also suggested that graphitic nitrogen is more important for the electrocatalytic activity of nitrogen-doped carbon.[35] Our XPS results indicate that N-graphene contains all these three functional groups (pyridinic-N, pyrrolic-N, and graphitic-N). It is believed that carbon atoms adjacent to nitrogen dopants possess a substantially higher positive charge density to counterbalance the strong electronic affinity of the nitrogen atom,[29] which results in an enhanced adsorption of O_2 and reactive intermediates (i.e., superoxide, hydroperoxide) that proceeds to accelerate the ORR.[36-38] The nitrogen-induced charge delocalization could also change the chemisorption mode of O_2 from monoatomic end-on adsorption on undoped carbon to a diatomic side-on adsorption at nitrogen functionalized carbon structure which effectively weakens the O–O bond to facilitate ORR.[29] This is also true for H_2O_2 reduction because breaking the O–O bond is also a key step for electrocatalytic reduction of H_2O_2. In addition, the presence of nitrogen in the structure enhances the ability of graphene sheets to donate electrons,[33] which is advantageous for reduction reactions.

SEM was employed to examine how electric filed can change the morphology of PNGs in the prepared electrocatalyst electrodes. Without inducement of the electric field, PNG aggregates dispersed randomly as shown in Figure 4(a) taken from surface of the electrode. Figures 4(c) and 4(e) show the

cross section images indicating the presence of aggregations in the sample without an electric field. Figure 4(b) exhibits the morphology of the PNG sample after applying 53.3 V/mm AC electric field. A smoother, more uniform and compact electrode surface can be seen (Figure 4(b)) after applying the electric field in the fabrication of electrocatalyst electrode, than the one without applying an electric field (see Figure 4(a)). The cross section SEM images of the sample in Figure 4(d) and (f) indicated layered structures formed by PNG aggregations, which parallel to each other. It is seen that PNGs were oriented with their flakes perpendicular to the applied electric field. This observed result is different from the previous reported one for the graphene flakes in epoxy nanocomposites, which showed most of the graphene nanoplatelets (GnPs) are aligned nearly parallel to the applied electric field direction.[19,20,39] The difference may be first due to that our PNGs are partially nitrogen functionalized graphene oxide sheets, which have a large number of positive and negative ions on the basal planes, including nitrogen, oxygen, OH and other groups on the graphene (carbon) nanosheets. The presence of these functional groups on both sides of graphene nanosheets can create polarized nano sheets in the electric field. The polarization of the PNG sheets via an external electric field induces an electrostatic Coulomb attraction causing the PNG layers approaching together to make a compacted subject and surface, as we can see from Figure 4(b) and (d). Secondly, the polymer used in the catalyst ink was Nafion solution, which is an electrolyte or ionomer, and is electric conductive; on the contrary, the epoxy solution used in the previous work was an insulator. Third, the PNGs loading in our catalyst ink is 99 wt%, which is much higher than those in previously reports such as in Reference [39], i.e., 0.27, 0.54, 0.81, and 1.08 vol% of graphene nanoplatelets (GnPs) in epoxy polymer.

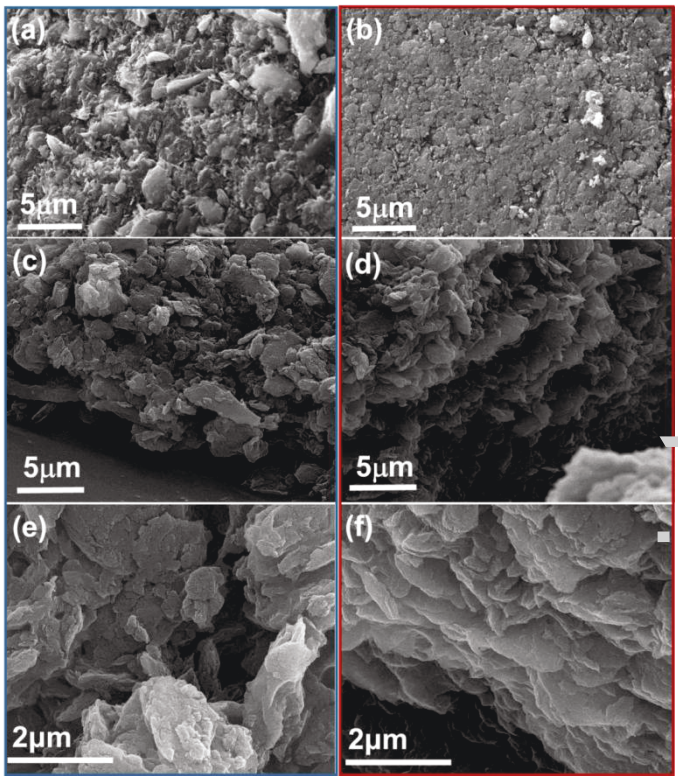

Figure 4. Blue box (left side): SEM images of PNGs without any applied AC electric field, (a) from its surface, (c) and (e) from its cross sections. Red box (right side): SEM images of PNGs [53.3 V/mm], (b) from its surface, (d) and (f) from its cross sections.

Applying an electric field to the PNGs in ethanol-Nafion based solution induces the orientation of graphene nano sheets from a random state to a nearly aligned state perpendicular to the electric field. In the presence of an electric filed, each PNG undergoes a polarization. Several mechanisms influence the material: (a) electric dipoles induced on PNGs; (b) field-induced torque on the dipoles; (c) dipole-dipole attraction; and (d) spatial redistribution of PNGs in applied field.[19] The dipole moments induced on PNGs cause the sheets to rotate, orient and move towards each other. Nitrogen functionalized graphene sheets are decorated with nitrogen, oxygen, hydrogen groups on both sides. These groups with different electronegativity on the graphene sheets have the tendency to be oriented along the electric field that induces polarized electric moments (dipoles). The polarization moment can be divided into two contributing components, i.e., one parallel to the flake ($p_{\parallel}$) and one perpendicular to the flake ($p_{\perp}$). For N-functionalized graphene, the polarization moment perpendicular to the flake is much larger than that parallel to the flake due to the application of an electric field. This

10.1002/ente.201800327

polarization moment leads to a field-induced torque T acting on the flake which is given by $T = p \times E$. In addition to electric field induced torque, Columbic attraction is another force that acts on the PNGs, which generated between the oppositely charged groups of neighbouring sheets. Under an AC electric field, dielectrophoresis movement of particles in a fluid under the influence of an electric field can occur.[40] Especially for PNGs, which are decorated with charged functional groups on both sides, electrostatic force between graphene nano-sheets can be more pronounced than those of non-charge particles. As a result, the polarized graphene sheets are able to migrate, rotate, orient, and move towards each other, as depicted in Figure 5. Furthermore, this Columbic attraction can cause the PNGs to be adjacent to each other to produce a firmly packed layer (Figure 5(d) & Figure 4). The PNGs are then stretched across the electrodes to provide an enhanced conductivity throughout the sample due to the applied electric field.

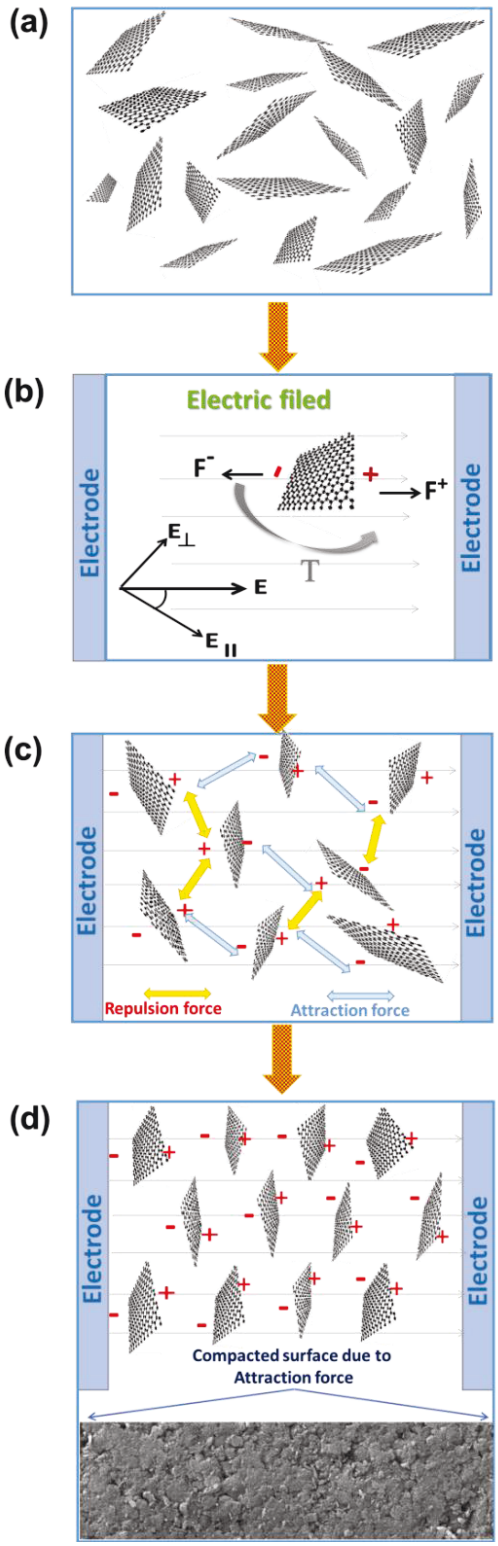

Figure 5. Schematics for the PNGs network forming process: (a) randomly PNGs; (b) electrical polarization and alignment. Polarization moment leads to a field-induced torque T acting on the flake; (c) interaction between aligned PNGs; (d) PNGs move close together and form network of aligned sheets. The mutual attractive or repulsive forces between two or more closely spaced sheets are due to the dielectric moments induced by an external electric field.

3.2. ORR Performance

We compared the performance of our samples for ORR catalysis in alkaline media (0.1 M KOH) saturated in O_2 using LSV. Comparing LSV data of GO and PNGs samples revealed that the presence of nitrogen can enhance the electrocatalytic performance, i.e., higher current density and more positive onset for PNGs than that of GO (Figure 6 (a)). Yang et al. [41] has showed that the presence of graphitic N (N-bonded to three carbon atoms) atoms which have relatively low energetic barrier for donating electrons from the surface of the catalyst can be responsible for ORR. Interestingly, after applying 53.3 V/mm AC electric field on the catalyst, a drastic improvement for ORR can be seen for PNGs (Figure 6(a)). Herein, PNGs [53.3 V/mm] in Figure 6 (a) refers to the sample after applying an electric field 53.3 V/mm.

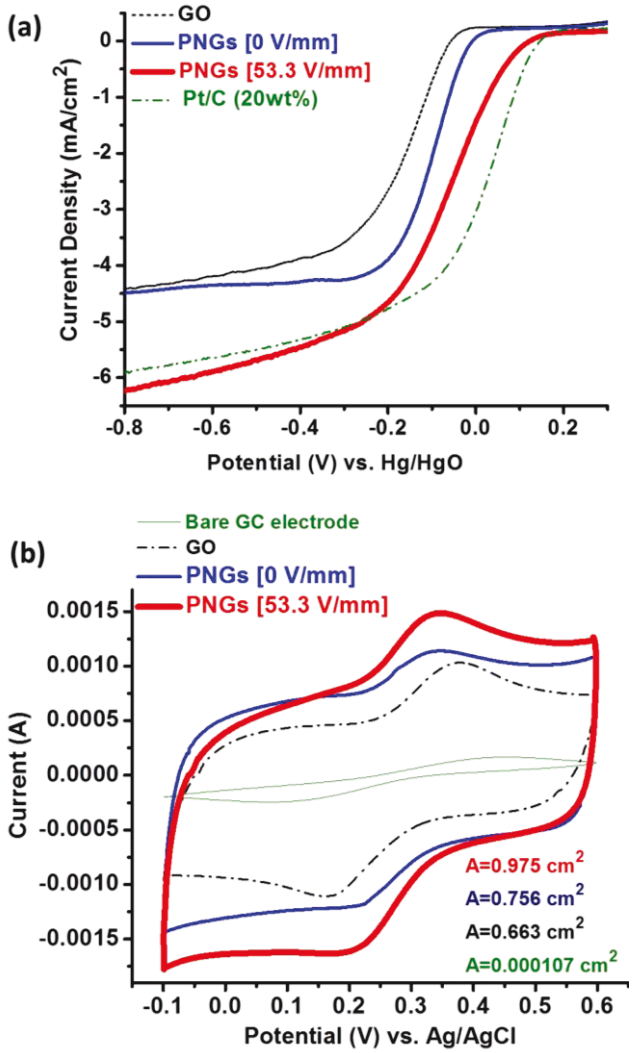

Figure 6. (a) LSV of GO, PNGs [0 V/mm], PNGs [53.3 V/mm], and Pt/C. (b) The electro active surface areas of different samples based on Randles-Sevcik equation for redox reactions involving Fe $(CN)_6^{3-/4-}$ in 10 mM $Fe(CN)_6^{3-/4-}$/1 M KCl.

The electroactive surface area of PNGs [53.3 V/mm] and PNGs [0 V/mm] were examined by studying the redox reactions involving $Fe(CN)_6^{3-/4-}$ (Figure 6(b)) using the CV measurements of two samples performed in 10 mM $Fe(CN)_6^{3-/4-}$ /1 M KCl. The electroactive surface area can be calculated based on the Randles-Sevcik equation:[42]

$$i_p = 2.99 \times 10^5 \, n \, A \, C \, D^{1/2} \, v^{1/2}$$

where i_p, n, A, C, D and v are the peak current, the number of electrons involved in the reaction, the electroactive surface area, the concentration of the reactant, the diffusion coefficient of the reactant species, and the scan rate, respectively. The redox reaction of $Fe(CN)_6^{3-/4-}$ involves one-electron transfer (n =1), and the diffusion coefficient (D) is 6.30 $\times 10^{-6}$ cm^2 s^{-1}. The electroactive surface area for PNGs [53.3 V/mm] is 0.975 cm^2, which is about 29% higher than that for PNGs [0 V/mm] at 0.756 cm^2. The electroactive surface area for PNGs [53.3 V/mm] is also larger than the other samples. Moreover, the charging process of the double layer capacitance at the working electrode is depicted by the current profile of the cycle. Figure 6(b)) shows the oxidation and reduction processes are facilitated after using PNGs [53.3 V/mm]. This indicates a strong enhancement of the effective electrode area. After applying different AC electric field values from 0 to 53.3 V/mm, LSV data of the PNG samples show a very promissing inhancement after applying 53.3 V/mm AC field, with respect to the onset potential (the potential at which a sharp increasing in the reduction current density occurs) as well as the current density compared to Pt/C catalyst as shown in Figure 7. The improvement of the onset potential after applying AC electric field of 53.3 V/mm on PNGs is about 0.2 V (i.e., changing from -0.1 V for PNGs [0 V/mm] to 0.1 V after using PNGs [53.3 V/mm], which is attributed to a better conductivity of the sample in this potential region. Applying an electric field higher than 53.3 V/mm can cause an aggregation of the PNGs to the middle of the electrode surface and reduce the electrical activities (Figure 8(c)). In the preparation of the catalyst electrode for measurement, although the GC electrode surface was totally covered by the catalyst ink, however, after applying an electric field higher than 53.3 V/mm, the aggregation of the catalyst powders occurred.

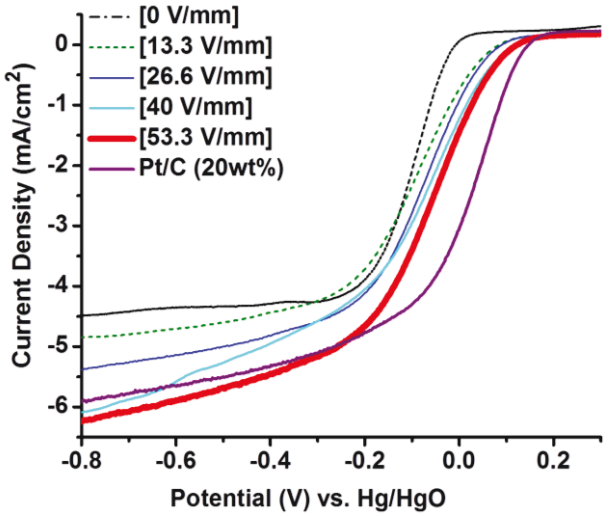

Figure 7. Comparison of LSV of Pt/C to PNGs after applying different AC-electric field for PNGs.

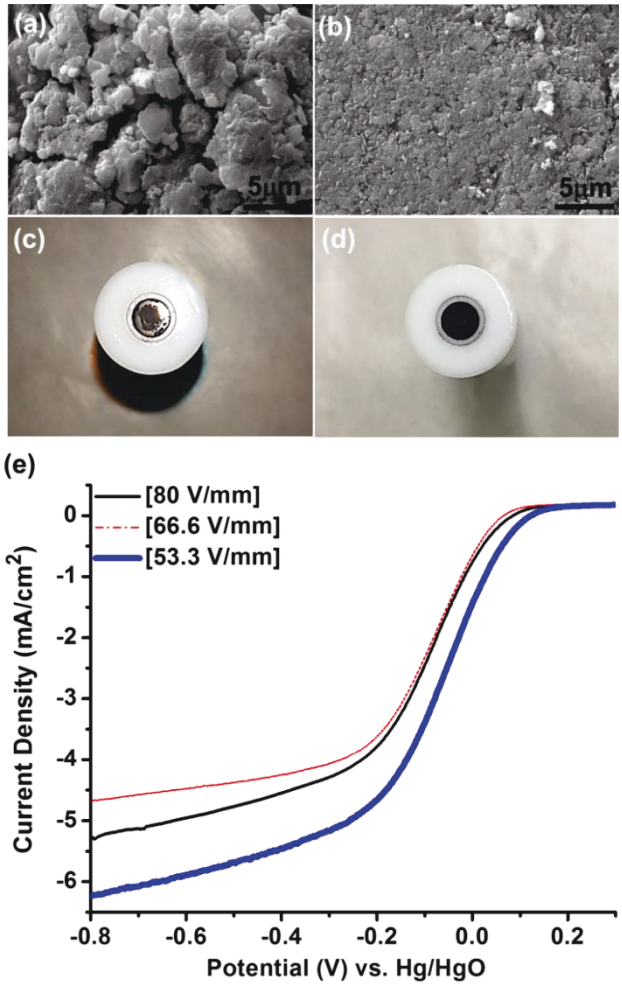

Figure 8. SEM images of (a) N-doped graphene after applying 80 V/mm AC, (b) 53.3 V/mm AC, (c) the image of the electrode surface corresponding to the sample (a). (d) The image of the electrode surface corresponding to the sample (b). (e) LSV of PNGs after applying high electric field. It seems after applying electric field higher than 53.3 V/mm, we have aggregation of the sample in the middle of the GC surface. That is why the electrical performance decreases.

The response of PNG sheets in an electric field is further studied from the differential conductance data, which were calculated as the differential of the current density in the material with respect to the applied potential that causes the current flow (Figure 9). Especially, there is a substantial enhancement of the differential conductance in PNGs [53.3 V/mm] sample for the potential region from -0.05 V to +0.2 V, in comparison with that of PNGs [0 V/mm] sample. As we can see in Figure 9, the differential conductance of PNGs [53.3 V/mm] is shifted towards that of Pt/C by around 0.1 V, indicating a better conductivity of the sample to exhibit a better electrochemical performance. As mentioned above, The polarization of the PNGs sheets allow for the manipulation of sheet orientation under the electrical field due to the dielectrophoresis effect among the dispersed individual sheets, which led to a uniform and compact electrode surface with a better conductivity. The extraction of the differential conductance from the LSV data can be a new approach for the electrochemical studies without performing additional experiments and instruments.

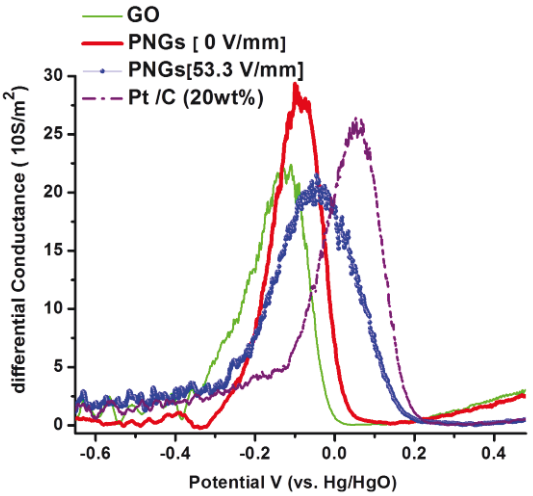

Figure 9. Comparison of differential conductances (in 10 S/m^2) of different PNG samples after applying different AC electric field and the result of Pt/C (20wt %) sample.

The Tafel equation describes the electrochemical kinetics relating the rate of an electrochemical reaction to the overpotential.[43] Larger Tafel slope indicates that a larger resistance (or a large loss of potential) is necessary to accelerate a chemical reaction. Figure 10(d) shows that the sample PNGs [53.3 V/mm] exhibits smaller Tafel slopes for ORR comparable to that of PNGs [0 V/mm].

In order to understand the number of electrons involved in the reaction, Koutecky–Levich plots were used (Figure 10(b) & (c)). The corresponding Koutecky–Levich plots (j^{-1} vs. (rotation speed, ω)$^{-1/2}$) at various electrode potentials show good linearity for PNGs [53.3 V/mm]. Linearity and parallelism of both plots are considered as typical of first-order reaction kinetics with respect to the concentration of dissolved O_2 (Figure 10(b)). ORR occurs either *via* a direct 4-electron reduction pathway where O_2 is reduced to H_2O, a 2-electron reduction pathway where it is reduced to hydrogen peroxide (H_2O_2), or an indirect 4-electron reduction pathway where the generated H_2O_2 is further reduced to H_2O. The numbers of electrons transferred at potential from -0.9 V to -0.3V for PNGs [53.3 V/mm] are shown in Figure 10(f). Thus, the sample prepared using an AC electric field 53.3 V/mm showed a better activity for ORR compared to other samples, forming around 4 electrons during the ORR. The partially reduced O_2 can further reacted with H^+ and produce two water molecules via the 4 electron transfer pathway without any activation energy barrier, which is more practical for industrial applications. In addition, the pyridinic-type sites on the open edges of PNGs [53.3 V/mm] can also contribute to the catalytic activity for ORR. Yang et al. [41] recently showed that the presence of graphitic N (N-bonded to three carbon atoms) group which has a relatively low energetic barrier for donating electrons from the catalyst surface in ORR. The quaternary N atoms in graphene-type structure could give electrons to the π-conjugated system and increase nucleophile strength of the adjacent carbon rings [C (δ^-)] that improves O_2 adsorption.

The durability of PNGs [53 V/mm] sample as ORR catalyst was also evaluated against PNGs [0 V/mm] electrode. The tests were performed using chrono-amperometry in 0.1M KOH solution saturated with O_2 (see Figure 10(e)). The corresponding current–time chrono-amperometric response of PNGs [53.3 V/mm] exhibited a very slow attenuation with only about 13% reduction for ORR region over 8,000 seconds; in comparison, PNGs [0 V/mm] showed about 26% reduction in ORR region. The electrochemical properties of these PNGs are comparable with nitrogen doped carbon or nanocarbon materials reported in the literature.[44-47]

4. Conclusion

Partially nitrogen-functionalized graphene nanosheets were synthesized by annealing the sample in ammonia solution for 12 h at 220^{o}C. This method has enhanced ORR activity in PNGs via the implantation of nitrogen active sites. A new method for preparing PNG nano-sheets oriented by an electric field for electrocatalytic electrode is reported. The origination of graphene sheets *via* applying AC electric field aligned them parallel to the electrode surface. PNGs [53.3 V/mm] sample showed the best performance indicating smaller overpotential, comparable to Pt/C, among the samples. The enhancement of electrochemical performance was a result of the polarization on N-functionalized graphene nanosheets, which caused a dielectrophoresis phenomenon. It produced a compact electrocatalytic electrode which can serve a better conductance with a good stability in alkaline electrolytes. The large accessible oriented nano sheets with high electrical conductivity make this low cost catalyst a superior electrode material for various energy storage/conversion device applications. Developing highly efficient electrocatalysts to facilitate sluggish cathodic oxygen reduction reaction is a key issue for metal-air batteries and fuel cells. This new physical approach for producing oriented materials for electrochemical applications can be used for mass production of electrocatalysts for green energy technology applications.

Acknowledgments

The work was funded in part by the Army Research Office (ARO) (Award No W911NF-15-1-0483) and the National Science Foundation (NSF) CREST project (Award No HRD 1736136) in the United States.

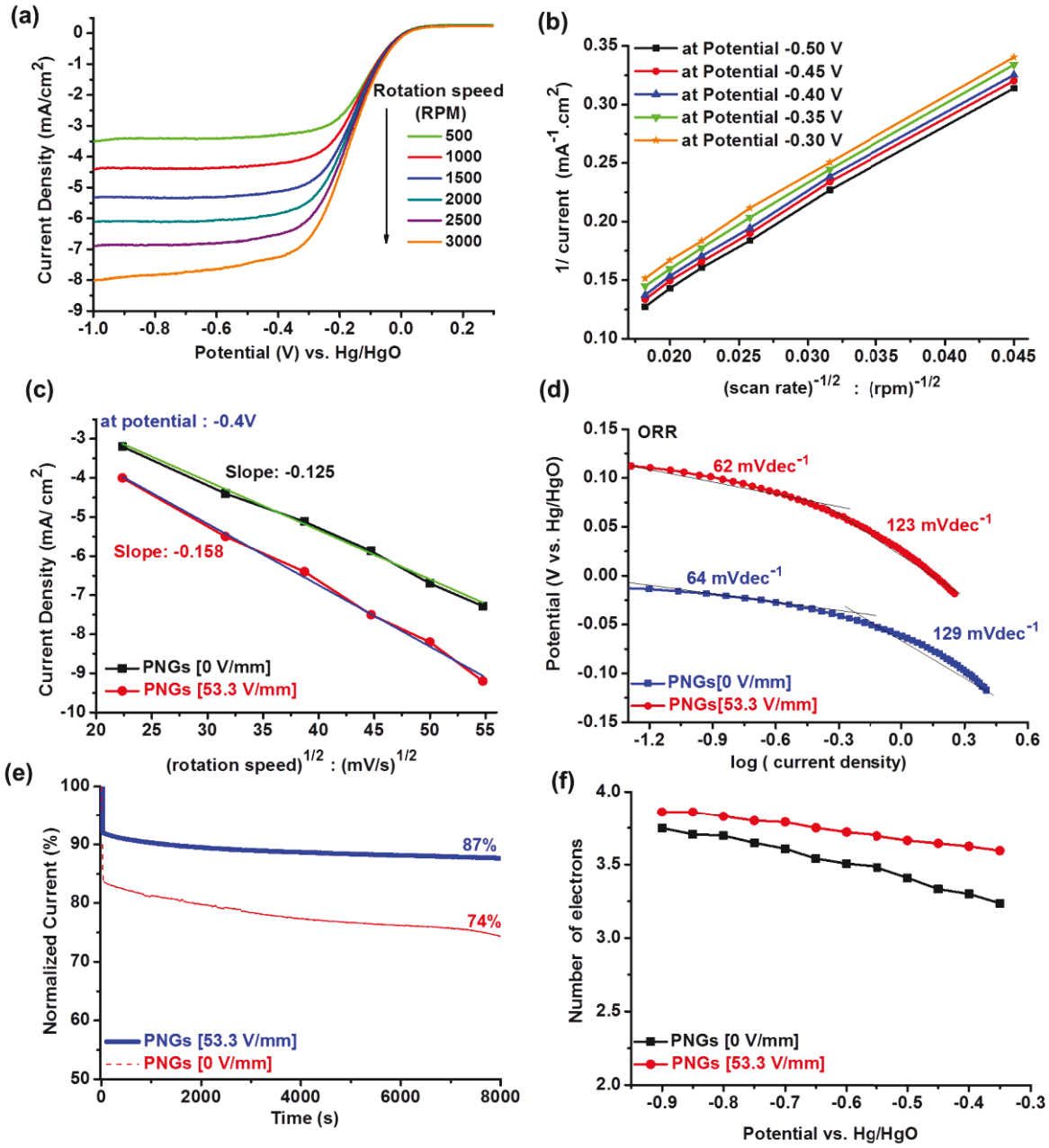

Figure 10. (a) Hydrodynamic voltammograms of PNGs in O_2-saturated 0.1 M KOH solution with various rotation rates from 500 to 3000 rotation *per minute* (rpm) at a scan rate of 10 mV/s. **(b)** Koutecky–Levich plots at different electrode potentials related to ORR region. (c) Koutecky–Levich plots at -0.4V for PNGs [53.3 V/mm] and PNGs [0 V/mm]. (d) Tafel slopes of PNGs [53.3 V/mm] and PNGs [0 V/mm] in ORR region. (**e)** Durability Test: Current-time chrono-amperometric responses of PNGs [53.3 V/mm] and PNGs [0 V/mm] on a GC electrode performed in O_2-saturated 0.1 M KOH. The percentages are the reference to the initial current at time zero. (f) The number of electrons involved in the reaction for PNGs [53.3 V/mm] and PNGs [0 V/mm].

References:

[1] Novoselov, K. S.; Geim, A. K.; Morozov, S. V.; Jiang, D.; Zhang, Y.; Dubonos, S. V.; Grigorieva, I. V.; Firsov, A. A. *Science* **2004**, *306*, 666.

[2] Novoselov, K. S.; Geim, A. K.; Morozov, S. V.; Jiang, D.; Katsnelson, M. I.; Grigorieva, I. V.; Dubonos, S. V.; Firsov, A. A. *Nature* **2005**, *438*, 197.

[3] Zhang, Y. B.; Tan, Y. W.; Stormer, H. L.; Kim, P. *Nature* **2005**, *438*, 201.

[4] Avouris, P. *Nano Lett.* **2010**, *10*, 4285.

[5] Chen, J. H.; Jang, C.; Xiao, S. D.; Ishigami, M.; Fuhrer, M. S. *Nat. Nanotechnol.* **2008**, *3*, 206.

[6] Mayorov, A. S.; Gorbachev, R. V.; Morozov, S. V.; Britnell, L.; Jalil, R.; Ponomarenko, L. A.; Blake, P.; Novoselov, K. S.; Watanabe, K.; Taniguchi, T.; Geim, A. K. *Nano Lett.* **2011**, *11*, 2396.

[7] Gong, K. P.; Du, F.; Xia, Z. H.; Durstock, M.; Dai, L. M. *Science* **2009**, *323*, 760.

[8] Wang, Q.; Dai, J. F.; Li, W. X.; Wei, Z. Q.; Jiang, J. L. *Compos. Sci. Technol.* **2008**, *68*, 1644.

[9] Monti, M.; Natali, M.; Torre, L.; Kenny, J. M. *Carbon* **2012**, *50*, 2453.

[10] Ma, C.; Zhang, W.; Zhu, Y. F.; Ji, L. J.; Zhang, R. P.; Koratkar, N.; Liang, J. *Carbon* **2008**, *46*, 706.

[11] Jiao, W. C.; Shioya, M.; Wang, R. G.; Yang, F.; Hao, L. F.; Niu, Y.; Liu, W. B.; Zheng, L.; Yuan, F.; Wan, L.; He, X. D. *Compos. Sci. Technol.* **2014**, *99*, 124.

[12] Yan, H. Y.; Tang, Y. X.; Long, W.; Li, Y. F. *J. Mater. Sci.* **2014**, *49*, 5256.

[13] Wu, S. Y.; Ladani, R. B.; Zhang, J.; Kinloch, A. J.; Zhao, Z. H.; Ma, J.; Zhang, X. H.; Mouritz, A. P.; Ghorbani, K.; Wang, C. H. *Polymer* **2015**, *68*, 25.

[14] Prasse, T.; Cavaille, J. Y.; Bauhofer, W. *Compos. Sci. Technol.* **2003**, *63*, 1835.

[15] Schwarz, M. K.; Bauhofer, W.; Schulte, K. *Polymer* **2002**, *43*, 3079.

[16] Wu, S. Y.; Ladani, R. B.; Zhang, J.; Bafekrpour, E.; Ghorbani, K.; Mouritz, A. P.; Kinloch, A. J.; Wang, C. H. *Carbon* **2015**, *94*, 607.

[17] Wang, H.; Zhang, H.; Zhao, W.; Zhang, W.; Chen, G. *Compos. Sci. Technol.* **2008**, *68*, 238.

[18] Kim, G.; Shkel, Y. M. *J. Mater. Res.* **2004**, *19*, 1164.

[19] Kim, G. *Compos. Sci. Technol.* **2005**, *65*, 1728.

[20] Wang, H. Q.; Zhang, H. Y.; Chen, G. H. *Compos. Pt. A-Appl. Sci. Manuf.* **2007**, *38*, 2116.

[21] Chen, G. H.; Wang, H. Q.; Zhao, W. F. *Polym. Adv. Technol.* **2008**, *19*, 1113.

[22] Wang, H. Q.; Zhang, H. Y.; Zhao, W. F.; Zhang, W.; Chen, G. H. *Compos. Sci. Technol.* **2008**, *68*, 238.

[23] Kincaid, D. R.; Cheney, E. W. *Numerical analysis: mathematics of scientific computing*; American Mathematical Soc., 2002; Vol. 2.

[24] Li, J.; Lin, H.; Yang, Z.; Li, J. *Carbon* **2011**, *49*, 3024.

[25] Li, J.; Liu, C.-y.; Liu, Y. *J. Mater. Chem.* **2012**, *22*, 8426.

[26] Cui, P.; Lee, J.; Hwang, E.; Lee, H. *Chem. Commun.* **2011**, *47*, 12370.

[27] Ouyang, W.; Zeng, D.; Yu, X.; Xie, F.; Zhang, W.; Chen, J.; Yan, J.; Xie, F.; Wang, L.; Meng, H. *Int. J. Hydrogen Energy* **2014**, *39*, 15996.

[28] Du, D.; Li, P.; Ouyang, J. *ACS Appl. Mater. & interfaces* **2015**, *7*, 26952.

[29] Gong, K.; Du, F.; Xia, Z.; Durstock, M.; Dai, L. *Science* **2009**, *323*, 760.

[30] Shao, Y.; Sui, J.; Yin, G.; Gao, Y. *Appl. Catal., B* **2008**, *79*, 89.

[31] Shao, Y.; Zhang, S.; Engelhard, M. H.; Li, G.; Shao, G.; Wang, Y.; Liu, J.; Aksay, I. A.; Lin, Y. *J. Mater. Chem.* **2010**, *20*, 7491.

[32] Matter, P. H.; Zhang, L.; Ozkan, U. S. *J. Catal.* **2006**, *239*, 83.

[33] Kundu, S.; Nagaiah, T. C.; Xia, W.; Wang, Y.; Dommele, S. V.; Bitter, J. H.; Santa, M.; Grundmeier, G.; Bron, M.; Schuhmann, W. *J. Phys. Chem. C* **2009**, *113*, 14302.

[34] Arrigo, R.; Hävecker, M.; Schlögl, R.; Su, D. S. *Chem. Commun.* **2008**, 4891.

[35] Niwa, H.; Horiba, K.; Harada, Y.; Oshima, M.; Ikeda, T.; Terakura, K.; Ozaki, J.-i.; Miyata, S. *J. Power Sources* **2009**, *187*, 93.

[36] Maldonado, S.; Stevenson, K. J. *J. Phys. Chem. B* **2005**, *109*, 4707.

[37] Gao, F.; Zhao, G.-L.; Yang, S. *ACS Catal.* **2014**, *4*, 1267.

[38] Gao, F.; Zhao, G.-L.; Wang, Z.; Bagayoko, D.; Liu, D.-J. *Chem. Commun.* **2015**, *62*, 79.

[39] Wu, S.; Ladani, R. B.; Zhang, J.; Bafekrpour, E.; Ghorbani, K.; Mouritz, A. P.; Kinloch, A. J.; Wang, C. H. *Carbon* **2015**, *94*, 607.

[40] Thomas, Y.; Jones, B.; Cambridge University Press, Cambridge: **1995**.

[41] Yang, H. B.; Miao, J.; Hung, S.-F.; Chen, J.; Tao, H. B.; Wang, X.; Zhang, L.; Chen, R.; Gao, J.; Chen, H. M. *Science advances* **2016**, *2*, e1501122.

[42] Jahan, M.; Liu, Z.; Loh, K. P. *Adv. Funct. Mater.* **2013**, *23*, 5363.

[43] Bard, A. J.; Faulkner, L. R. *Electrochem. Methods* **2001**, *2*, 482.

[44] Gong, K.; Du, F.; Xia, Z.; Durstock, M.; Dai, L. *Science* **2009**, *323*, 760.

[45] Wohlgemuth, S.-A.; White, R. J.; Willinger, M.-G.; Titirici, M.-M.; Antonietti, M. *Green Chem.* **2012**, *14*, 1515.

[46] Lin, Z.; Waller, G.; Liu, Y.; Liu, M.; Wong, C. P. *Adv. Energy Mater.* **2012**, *2*, 884.

[47] Chen, Z.; Higgins, D.; Chen, Z. *Carbon* **2010**, *48*, 3057.